The magnetic properties of single-domain particles with cubic anisotropy. I. Hysteresis loops

1993 J. Phys.: Condens. Matter 5 2779

(http://iopscience.iop.org/0953-8984/5/17/012)

J. Phys.: Condens. Matter 5 (1993) 2779–2792. Printed in the UK

The magnetic properties of single-domain particles with cubic anisotropy: I. Hysteresis loops

M Walker†, P I Mayo†, K O'Grady†, S W Charles†, R W Chantrell‡

† Magnetic Materials Research Group, School of Electronic Engineering Science, UCNW Bangor, Gwynedd, LL57 1UT, UK

‡ Department of Physics, Keele University, Keele, Staffordshire, ST5 5BG, UK

Received 4 December 1992, in final form 19 February 1993

Abstract. A comprehensive study of the magnetic properties of non-interacting single-domain particles with cubic magnetocrystalline anisotropy is presented. These numerical calculations extend the zero-temperature predictions of Joffe and Heuberger and enable the effects of thermally activated magnetization reversal on the hysteresis loop at finite temperatures to be determined. Variations in particle size distribution are also considered. Calculations indicate a reduction in the intrinsic coercivity as the mean particle diameter is reduced and an increase in coercivity for small particle diameter systems as the standard deviation of the size distribution is increased.

1. Introduction

The first systematic calculations of hysteresis loop behaviour were performed on uniaxial fine-particle systems at zero temperature by Stoner and Wohlfarth in 1948 [1]. Subsequently, Gaunt [2] and Joffe [3] extended these studies by including the effects of non-zero temperatures on magnetization reversal.

Materials with multiaxial cubic anisotropy have also been the subject of hysteresis loop predictions, most notably by Joffe and Heuberger in 1974 [4]. Joffe and Heuberger predicted hysteresis loops for a system of identical non-interacting particles having cubic magnetocrystalline anisotropy with $K > 0$ (three easy axes along the cube edges) and $K < 0$ (four easy axes along the body diagonals). The Joffe and Heuberger treatment, however, does not account for thermal agitation, and irreversible behaviour would only occur in their model when the energy barrier vanishes due to the application of a sufficiently large applied field.

More recently Geshev and co-workers [5, 6] have reported theoretical predictions of the thermomagnetic properties and remanence curves of particle systems with cubic symmetry. These predictions introduce the effects of temperature through an implicit variation of the reduced field $h = I_s H/2|K|$ by adopting temperature-dependent variations in the saturation moment I_s and anisotropy constant K.

The concept of thermally activated magnetization reversal in fine-particle systems is well known [7]. These effects are more usually examined via calculations of the relaxation time for the phenomenon which is usually considered to follow an Arrhenius–Néel-type law [8]:

$$\tau^{-1} = f_0 \exp(-\Delta E/kT). \tag{1}$$

0953-8984/93/172779+14$07.50

A knowledge of the measurement time then enables the contribution of thermal activation to be assessed.

The effects of a distribution of particle sizes should also be taken into account to mirror the situation generally observed in real systems. Chantrell and co-workers [9] have reported the effects of a particle size distribution on the coercivity of uniaxial systems also taking into account the effects of thermal agitation.

In a subsequent paper, Chantrell and co-workers [10] have also shown that, for a system with easy axes aligned parallel to the applied field and a given particle size distribution at an appropriate temperature, three distinct types of behaviour can be observed in reverse fields following saturation.

For the smallest particles thermal fluctuations will enable spontaneous magnetization reversal or superparamagnetism [11] to occur, which can generally be described by the Langevin function.

For larger particles which are not superparamagnetic, magnetization reversal can occur due to a combination of thermal and field-induced effects. These particles are then blocked in the reverse field direction. The largest particles have their moments blocked in their original direction until a sufficiently large reverse field is applied.

The net magnetization is then the sum of the three integrals over differing parts of the size distribution. These magnetization components are shown schematically in figure 1.

In this paper we develop a model of a system of particles with cubic anisotropy at a finite temperature using the concept of the critical diameter.

2. The computer model

2.1. Basic model of Joffe and Heuberger

Adopting the coordinate system defined by Joffe and Heuberger [4] and illustrated in figure 2, the orientation of the axes of any particle relative to the applied field $-H$ may be expressed in terms of the angles (θ, ψ). The orientation of the magnetization vector of a particular particle may be similarly described, relative to the principal anisotropy axes, in terms of the angles (γ, ϑ). The total reduced free energy of such a particle containing a single domain

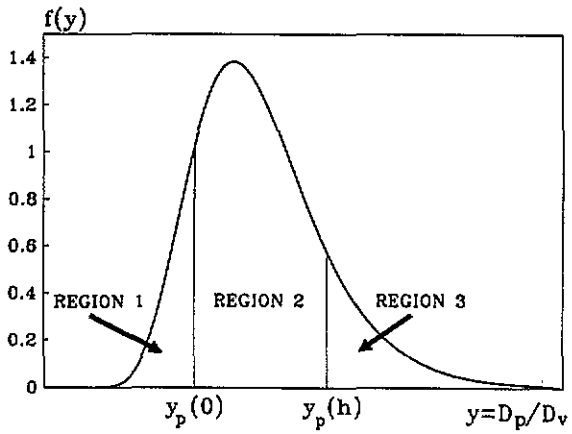

Figure 1. Schematic representation of the three distinct regions of magnetization reversal in a size-distributed particle system. This log-normal distribution also shows the typical positions for $y_p(0)$ and $y_p(h)$.

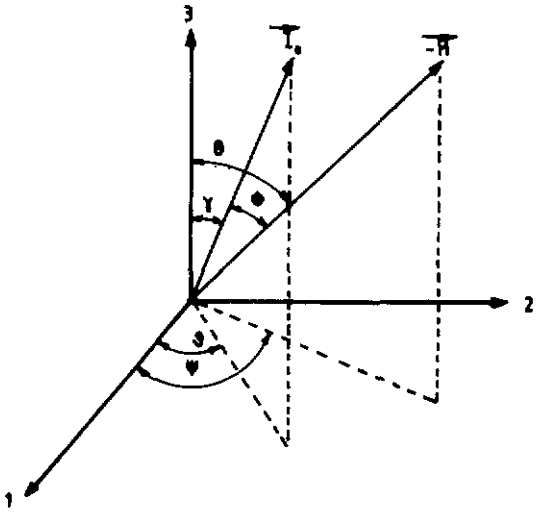

Figure 2. Definition of orientational angles relative to principal directions of the cube.

and exhibiting cubic magnetocrystalline anisotropy, neglecting demagnetization and surface effects, can be then written as

$$\eta(\gamma, \vartheta) = \frac{E}{2|K|V} = \frac{K}{2|K|}(\alpha_1^2\alpha_2^2 + \alpha_2^2\alpha_3^2 + \alpha_1^2\alpha_3^2) + h\cos\phi \tag{2}$$

where h is the reduced field ($= HI_s/2|K|$), I_s the saturation magnetization, E the total energy, V the particle volume, K the first-order anisotropy constant, α_1, α_2, α_3 are the direction cosines and $\cos\phi$ is given by

$$\cos\phi = \cos\gamma\cos\theta + \sin\gamma\sin\theta\cos(\vartheta - \psi). \tag{3}$$

The direction cosines are given by

$$\alpha_1 = \sin\gamma\cos\vartheta \qquad \alpha_2 = \sin\gamma\sin\vartheta \qquad \alpha_3 = \cos\gamma. \tag{4}$$

Therefore the dimensionless energy equation may be expressed as follows:

$$\eta(\gamma, \vartheta) = \frac{K}{2|K|}[\sin^2\gamma - \sin^4\gamma(1 - \tfrac{1}{4}\sin^2 2\vartheta)] + h[\cos\gamma\cos\theta + \sin\gamma\sin\theta\cos(\vartheta - \psi)]. \tag{5}$$

The set of values (γ, ϑ) that minimize the energy equation (5) represent the equilibrium orientations of the magnetization vector at that field and particle orientation value. It is possible to analytically determine the easy directions in zero applied field by setting h equal to zero and solving the partial differential equations for η, with respect to γ and ϑ, when set to zero. Further, calculation of the second derivatives will enable the nature of the solutions to be investigated and determine whether they are minima, maxima or saddle points.

When $K > 0$ there are six minima along the cube edges denoted by the axes 1, 2 and 3 and the corresponding reverse directions along these axes. Putting this in terms of Miller indices the equivalent directions would be [100], [010], [001], [$\bar{1}$00], [0$\bar{1}$0] and [00$\bar{1}$]. In zero applied field the six angle configurations that give the desired energy minima are

$$\gamma_{\min} = 0 \qquad \gamma_{\min} = \frac{\pi}{2} \qquad \gamma_{\min} = \pi$$

for each of

$$\vartheta_{\min} = [0, \pi] \qquad \vartheta_{\min} = 0, \frac{\pi}{2}, \pi, \frac{3\pi}{2} \qquad \vartheta_{\min} = [0, \pi].$$

Similarly, the maxima are at eight orientations of the type ⟨111⟩ along the body diagonals given by

$$\gamma_{\max} = \cos^{-1}(3^{-1/2}) \qquad \gamma_{\max} = \pi - \cos^{-1}(3^{-1/2})$$

for each of

$$\vartheta_{\max} = \frac{\pi}{4}, \frac{3\pi}{4}, \frac{5\pi}{4}, \frac{7\pi}{4}.$$

The saddle points are at twelve orientations of the type ⟨110⟩ along the face diagonals given by

$$\gamma_{\text{sdl}} = \frac{\pi}{4} \qquad \vartheta_{\text{sdl}} = 0, \frac{\pi}{2}, \pi, \frac{3\pi}{2}$$

$$\gamma_{\text{sdl}} = \frac{\pi}{2} \qquad \vartheta_{\text{sdl}} = \frac{\pi}{4}, \frac{3\pi}{4}, \frac{5\pi}{4}, \frac{7\pi}{4}$$

$$\gamma_{\text{sdl}} = \frac{3\pi}{4} \qquad \vartheta_{\text{sdl}} = 0, \frac{\pi}{2}, \pi, \frac{3\pi}{2}.$$

When $K < 0$ the maxima and minima values obtained for $K > 0$ are interchanged. Thus there are eight easy directions of the type ⟨111⟩ and six maxima of the type ⟨100⟩.

In the presence of an applied field however, the energy function (5) is much more difficult to minimize. Assume the sample is saturated in a large negative field. For $h < 2$ only one position of (γ, ϑ) is stable and located in the first octant. If h is reduced from this value to zero, the magnetization vector remains in the position of lowest energy. When a reverse field is applied, this energy minimum is raised, the equilibrium becomes metastable and, with increasing reverse field, unstable. The magnetization will swing out of the first octant, and it is here that a systematic approach must be introduced to determine the path leading to the relevant local minimum. The computer model employed two procedures to determine the orientations $\gamma_{\min}$ and $\vartheta_{\min}$ which give a true minimum energy. A steepest descent method is initially performed to give values of γ and ϑ close to the true minimum values, followed by a Newton–Raphson method, for functions of two variables, to rapidly converge to an accurate minimum.

The basic computational procedure is as follows.

(1) The anisotropy constant, K, is set.

(2) The reduced applied field, h, is started from $h = -10$ and is incremented in small steps to $+1$ and then to -1 to complete the full hysteresis loop. The size of field step varied, depending on the relative position of the hysteresis loop. Smaller field steps, $h_{\text{increment}} = 0.03$, were made during critical switching regions of the hysteresis loop compared to the more stable magnetic regions where switching was not likely to occur when $h_{\text{increment}} = 0.05$.

(3) The particle orientation angles (θ, ψ) are both incremented from 0 to $\pi/2$ in increments of $\pi/90$ at each value of the applied field.

(4) The steepest descent procedure is performed for each particle orientation at each field value. At the first field value of $h = -10$, for all particle orientations, the magnetization vector is approximately parallel to the applied field. Therefore, the starting values for this procedure are at $h = -10$ are $\gamma = \theta$ and $\vartheta = \psi$. The steepest descent procedure is terminated at the point where the gradient becomes zero.

(5) The Newton–Raphson method is started using the values of (γ, ϑ) output from the steepest descent procedure. At each orientation of (θ, ψ) the values of (γ, ϑ) are stored and used to initialize the steepest descent procedure for the same orientation (θ, ψ) in the next value of the field.

Therefore, completing steps 1–5 for all values of the applied magnetic field will enable a full set of the minimum values of the magnetization vector angles, $\gamma_{\min}$ and $\vartheta_{\min}$, to be determined for all the possible orientations of particle easy axis, (θ, ψ), and for all h.

2.2. *The introduction of temperature*

The process of magnetization reversal of single-domain particles in the absence of thermal agitation involves the application of an external applied field sufficiently large to overcome the energy barrier to reversal of the magnetization vector from one stable energy configuration to another. With the introduction of temperature the magnetization reversal process is activated by thermal energy. In particular, if the thermal energy is of sufficient magnitude an irreversible transition over the energy barrier may be thermally activated. The criterion for such a reversal is given by

$$T_{\text{red}} \geqslant \Delta\eta \tag{6}$$

where $\Delta\eta$ is the magnitude of the reduced energy barrier and T_{red} is the reduced temperature [2] given by

$$T_{\text{red}} = \frac{kT \ln(tf_0)}{2|K|V} \tag{7}$$

where f_0 is of the order of the Larmor precession frequency, taken to equal $10^9\,\text{s}^{-1}$ [8, 11].

Assuming a measurement time of $t = 100\,\text{s}$ results in

$$T_{\text{red}} = \frac{25kT}{2|K|V}. \tag{8}$$

For particles with cubic anisotropy the lowest point in their energy barrier occurs at the saddle point:

$$\Delta\eta = \eta(\gamma_{\text{saddle}}, \vartheta_{\text{saddle}}) - \eta(\gamma_{\min}, \vartheta_{\min}). \tag{9}$$

Thus if the inequality (6) is satisfied, the magnetization vector will overcome the energy barrier and move to a new local minimum.

In zero applied field, for $K > 0$, the reduced energy barrier is equal to 0.125 for all values of (θ, ψ), exactly one quarter of the magnitude of the energy barriers for the uniaxial particles [1]. Similarly, for $K < 0$ in zero applied field, the energy barrier is equal to $0.04166\dot{6}$ for all values of (θ, ψ), a factor twelve smaller than the equivalent uniaxial particle configuration. Thus

$$\Delta E = 2KV\Delta\eta = \frac{KV}{4} \qquad \text{for} \quad K > 0 \tag{10}$$

$$\Delta E = 2KV\Delta\eta = \frac{KV}{12} \qquad \text{for} \quad K < 0. \tag{11}$$

Therefore, the reduced temperature at which superparamagnetism manifests itself, for $K > 0$ and $K < 0$, will be $T_{\text{red}} = 0.125$ and $T_{\text{red}} = 0.04166\dot{6}$, respectively.

For the single-particle size case, additional steps are needed in the basic computational procedure to account for thermal effects. Since thermal transitions over the energy barriers will not take place until the reversing field has changed direction (i.e. when $h \leqslant 0$ for the

first quadrant of the loop and when $h \geqslant 0$ on the third quadrant of the loop), the following additional steps in the algorithm need only be performed on those portions.

(4a) $(\gamma_{\text{saddle}}, \vartheta_{\text{saddle}})$ are determined for all (θ, ψ) in the relevant portions of the hysteresis loop, starting at $h = 0$. It was found that only the Newton–Raphson procedure was required to accurately determine the saddle points. Using the sets of values of $(\gamma_{\text{min}}, \vartheta_{\text{min}})$ and $(\gamma_{\text{saddle}}, \vartheta_{\text{saddle}})$ the energy barriers are calculated at each value of (h, θ, ψ).

(6) If $T_{\text{red}} > \Delta\eta$, then the particle has made the transition into the reversing field direction. We then return to step 4 and redetermine $(\gamma_{\text{min}}, \vartheta_{\text{min}})$.

2.3. The inclusion of a particle size distribution

In real systems, the size of the particles varies over a certain range and has to be considered as a random variable of some statistical distribution. A particle within the distribution can be considered as either superparamagnetic or blocked, depending on the particle diameter.

Fine magnetic particle assemblies are frequently observed to possess a log-normal particle size distribution [9]. The most convenient form of a distribution is one of volume fraction $f(y)$, defined in terms of the reduced diameter $y = D/D_{\text{v}}$, where D_{v} is the median diameter of the system. Thus $f(y)\,\text{d}y$ is the fraction of the total volume of the particles having reduced diameters between y and $y + \text{d}y$.

The distribution shown in figure 1 indicates the three critical regions associated with a distributed system of magnetic fine particles. The particles in region 1 with $y < y_{\text{p}}(0)$ are superparamagnetic. Given that for thermal relaxation $\Delta E \leqslant 25kT$ [11] and that in zero field $\Delta E = KV/4$ where $K > 0$, the critical diameter for superparamagnetic behaviour, $D_{\text{p}}(0)$, is given by

$$D_{\text{p}}(0) = \left(\frac{600kT}{\pi K}\right)^{1/3}. \tag{12}$$

By rearranging (10) we may obtain an expression for $\Delta\eta$ in terms of the critical superparamagnetic volume in zero field, $V_{\text{p}}(0)$ and in applied field h, $V_{\text{p}}(h)$, where

$$\Delta\eta = \frac{\Delta E}{2KV_{\text{p}}(h)} = \frac{V_{\text{p}}(0)}{8V_{\text{p}}(h)}. \tag{13}$$

This expression may then be re-written in terms of the critical reduced diameter in applied field h, $y_{\text{p}}(h) = D_{\text{p}}(h)/D_{\text{v}}$, and the critical reduced diameter in zero field, $y_{\text{p}}(0) = D_{\text{p}}(0)/D_{\text{v}}$ where D_{v} is the median particle diameter:

$$y_{\text{p}}(h) = \frac{y_{\text{p}}(0)}{(8\Delta\eta)^{1/3}} \tag{14}$$

where the field dependence is included via $\Delta\eta$ given by (5) and (9).

Assuming the particles are initially in a large negative field, the tendency is for the magnetization vector to lie parallel to the field direction and the relevant orientation (γ, ϑ), minimizing the energy η and being located in the first octant. As h becomes increasingly positive it is possible for some of the magnetization vectors to make an irreversible transition over the energy barrier.

However, the largest particles in the third region of figure 1 where $y > y_{\text{p}}(h)$, continue to be blocked, due to their size, and cannot make the transition over their respective energy barriers. Only the smaller blocked particles, in region 2 of the distribution where $y_{\text{p}}(0) < y < y_{\text{p}}(h)$, can overcome the anisotropy energy barriers and their magnetization vectors can rotate into the direction of the positive field.

Thus, by calculating $y_p(0)$ and $y_p(h)$ it is possible to determine the fraction of the assembly that consists of superparamagnetic particles, blocked particles that have made the transition into the reversing field direction and blocked particles that remain in the saturating field direction.

3. Predictions of the single-particle volume model

3.1. Hysteresis at T = 0

Hysteresis loops at 0 K were evaluated using the computational methods outlined in section 2 by minimizing the values of γ_{min} and ϑ_{min} for all (θ, ψ). Assuming a random orientational distribution of crystalline axes, the number of particles per unit volume of the assembly having θ in the interval $(\theta, \theta + d\theta)$ and ψ in the interval $(\psi, \psi + d\psi)$ will be

$$dn(\theta, \psi) = \frac{2n}{\pi} \sin\theta d\theta d\psi \tag{15}$$

where n is the number of particles per unit volume of the assembly. In (15), the angles θ and ψ can take all values in the closed interval $[0, \pi/2]$, since all other orientations have symmetrical equivalents within this range. The reduced magnetization of an assembly of spherical single-domain particles with random orientated easy axes is then given by

$$\bar{I} = \frac{I}{I_s} = -\frac{2}{\pi} \int_0^{\frac{\pi}{2}} \int_0^{\frac{\pi}{2}} \left[\cos\gamma \cos\theta + \sin\gamma \sin\theta \cos(\psi - \vartheta)\right] \sin\theta d\theta d\psi. \tag{16}$$

Using (16), hysteresis loops were then computed for anisotropy constant values $K > 0$ or $K < 0$, the results of which are illustrated in figure 3. When K is positive the reduced coercivity ($h_c = H_c/H_K$, where H_K is the anisotropy field) is 0.321, much larger than when K is negative ($h_c = 0.189$). Similarly, the saturation remanence is slightly smaller for $K > 0$ $(\bar{I}_r = 0.831)$ than for $K < 0$ $(\bar{I}_r = 0.866)$. The shape and magnitude of both of these hysteresis loops is independent of particle diameter, since $T = 0$. These results agree exactly with those of Joffe and Heuberger [4] at 0 K, and implies that both models are operating correctly.

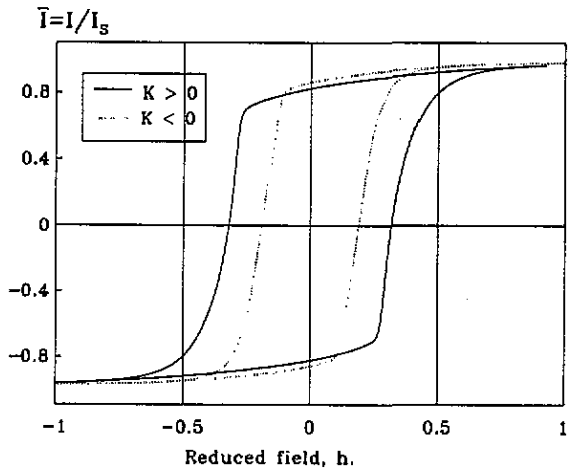

Figure 3. The hysteresis loops at $T = 0$ K for a system with $K > 0$ and $K < 0$.

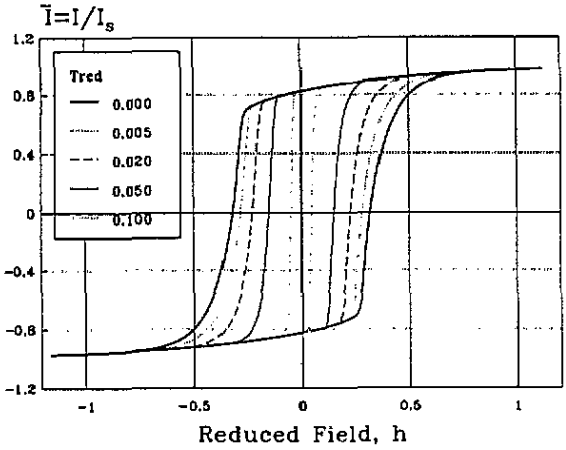

Figure 4. Hysteresis loops for a system of identical multiaxial particles as a function of reduced temperature, $K > 0$.

3.2. Hysteresis at $T \neq 0$

At 0 K, the first particle to make an irreversible rotation over the energy barrier is the particle with orientation ($\theta = 0°$, $\psi = 45°$) in a reverse field of $h = 0.274$. As the reduced temperature, T_{red}, is increased the magnitude of the critical field, h_0, (i.e. the field at which the first particle reverses its magnetization vector), decreases. Specifically, for $T_{red} = 0.05$ the particle orientated at ($\theta = 0°$, $\psi = 45°$) makes an irreversible transition at a lower reverse field of $h = 0.116$. Following this calculation for the other particles and again integrating enables the magnetization at any field to be obtained.

The calculated hysteresis loops for $K > 0$ are illustrated in figure 4 at various values of the reduced temperature T_{red}. As T_{red} is increased, the reduced coercivity decreases from its maximum value of 0.321 as more particles traverse the energy barrier in lower applied fields due to thermal agitation. The case for $K < 0$ will be the subject of a future publication.

The relationship between the reduced coercivity, h_c, and the reduced temperature, T_{red}, is shown in figure 5. As the reduced temperature increases the coercivity decreases from its maximum value at 0 K and becomes zero when $T_{red} = 0.125$. This reduced temperature value ($T_{red} = 0.125$) corresponds to the temperature at which the multiaxial system becomes superparamagnetic (i.e. $\bar{I}_r$ and h_c are both equal to zero). For single-sized particle systems the saturation remanence is invariant with reduced temperature (for $T_{red} < 0.125$) and only goes to zero at the superparamagnetic critical diameter. The form of this data corresponds well with the previous calculations of Joffe [3] for systems of identical isolated particles with uniaxial anisotropy. In that instance, however, the maximum reduced coercivity, in 0 K, was 0.479 and the introduction of superparamagnetic behaviour and zero coercivity occurred at $T_{red} = 0.5$.

4. Predictions for a system with a particle size distribution

4.1. Hysteresis

The magnetization of a system of particles with a distribution of particle sizes may be

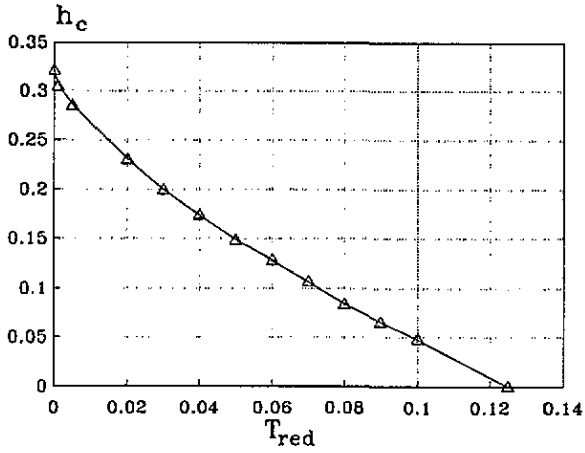

Figure 5. Effect of T_{red} on h_c for a system of identical multiaxial particles.

considered to consist of contributions due to those particles that are superparamagnetic and the larger particles that are blocked.

The reduced magnetization ($= I/I_s$) of the superparamagnetic particles $\bar{I}_1$ corresponding to region 1 of figure 1 is given by

$$\bar{I}_1 = \int_0^{y_p(0)} L(\alpha)\, f(y)\, dy \tag{17}$$

where $L(\alpha)$ is the Langevin function and $f(y)$ is the log-normal distribution of particle volume fraction represented by

$$f(y)\,dy = \frac{1}{\sigma\,(2\pi)^{1/2}\,y} \exp\left(-\frac{(\ln y)^2}{\sigma^2}\right) dy \tag{18}$$

where $y(= D/D_v)$ is the reduced particle diameter and D_v the median particle diameter. The standard deviation of the distribution is represented by σ.

The reduced magnetization of the blocked particles that have made the transition into the positive field direction (region 2 of figure 1) is given by

$$\bar{I}_2 = -\frac{2}{\pi} \int_0^{\frac{\pi}{2}} \int_0^{\frac{\pi}{2}} \left[\cos\gamma\cos\theta + \sin\gamma\sin\theta\cos(\psi - \vartheta)\right] F_{b1} \sin\theta\, d\theta\, d\psi \tag{19}$$

where

$$F_{b1} = \int_{y_p(0)}^{y_p(h)} f(y)\, dy. \tag{20}$$

The reduced magnetization of the blocked particles that remain in the negative field direction $\bar{I}_3$ (region 3 of figure 1) is given by

$$\bar{I}_3 = -\frac{2}{\pi} \int_0^{\frac{\pi}{2}} \int_0^{\frac{\pi}{2}} \left[\cos\gamma\cos\theta + \sin\gamma\sin\theta\cos(\psi - \vartheta)\right] F_{b2} \sin\theta\, d\theta\, d\psi \tag{21}$$

where

$$F_{b2} = \int_{y_p(h)}^{\infty} f(y)\, dy. \tag{22}$$

Therefore, the magnetization due to blocked particles at a value of field, h, is given by

$$\bar{I}_4 = \bar{I}_2 + \bar{I}_3. \tag{23}$$

Equation (19) is only applicable for $H < H_K$. However, if $H > H_K$ the equation describing the magnetization of a fine particle system where all the blocked particles have been rotated into the field direction, is

$$\bar{I}_4 = -\frac{2}{\pi}\int_0^{\frac{\pi}{2}}\int_0^{\frac{\pi}{2}}\left[\cos\gamma\cos\theta + \sin\gamma\sin\theta\cos(\psi - \vartheta)\right] F_{b3}\sin\theta\,d\theta\,d\psi \tag{24}$$

where

$$F_{b3} = \int_{y_p(0)}^{\infty} f(y)\,dy. \tag{25}$$

Thus, the total reduced magnetization of a system of independent cubic anisotropic particles with randomly oriented easy axes, assuming a log-normal particle size distribution, is given by the summation of the superparamagnetic particle contribution ($\bar{I}_1$) and the blocked particle contribution ($\bar{I}_4$):

$$\bar{I} = \bar{I}_1 + \bar{I}_4 \tag{26}$$

where the method of calculating $\bar{I}_4$ is dependent on the magnitude of H relative to H_K. If $H < H_K$ then $\bar{I}_4$ is calculated from (19) and (21) in (23), otherwise, when $H > H_K$, $\bar{I}_4$ is calculated from (24).

Following the inclusion of the above equations to our model, and adopting the method of Abramovitz and Stegun [12] to determine the distribution function integrals, the following hysteresis loops were numerically predicted.

Figure 6 shows the predicted hysteresis loops for the equivalent to a system of fine cobalt ferrite particles at a temperature of $T = 100\,\mathrm{K}$ and various median particle diameters (MPD); the standard deviation of the particle size distribution was kept constant at $\sigma = 0.3$. An anisotropy constant of $K = +2 \times 10^6\,\mathrm{erg\,cc^{-1}}$ and bulk saturation magnetization of $I_s = 400\,\mathrm{emu\,cc^{-1}}$ has been assumed. The superparamagnetic contributions to these hysteresis loops are illustrated in the associated figure 7.

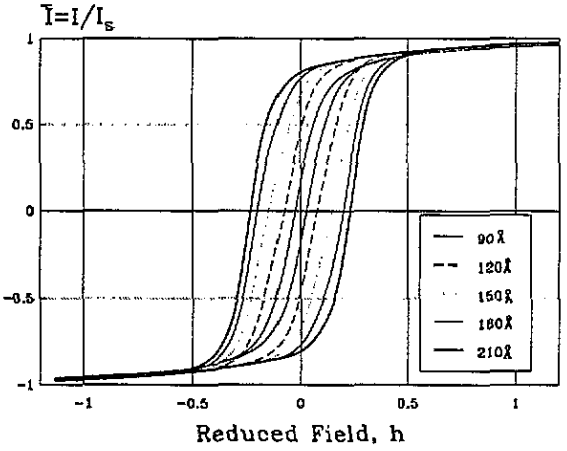

Figure 6. Hysteresis loops at 100 K for various values of median particle diameter where $\sigma = 0.3$, $K = 2 \times 10^6\,\mathrm{erg\,cc^{-1}}$ and $I_s = 400\,\mathrm{emu\,cc^{-1}}$.

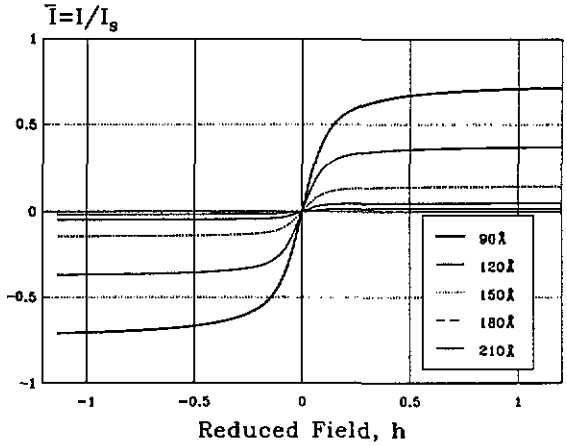

Figure 7. Superparamagnetic contributions to hysteresis loops at 100 K as a function of median particle diameter where $\sigma = 0.3$, $K = 2 \times 10^6$ erg cc^{-1} and $I_s = 400$ emu cc^{-1}.

Examination of the hysteresis loop for the smallest median diameter of 90 Å at 100 K indicates a substantial contribution to the magnetization from the superparamagnetic particles, and hence the maximum remanence observed at $T = 0$ K is not achieved at this temperature. For many applications of fine magnetic particles it is desirable to maintain a high remanence. One way of achieving this is by increasing the median diameter of the system. This effect is clearly shown in the hysteresis loops of figure 6, predicted with the same σ and median diameters up to 210 Å. As expected the remanence is substantially increased from 0.210 for the 90 Å system through to 0.811 for the 210 Å system. This latter value of remanence is close to the maximum remanence of 0.831 previously attained for the single-particle volume system when the superparamagnetic contribution was absent from the calculation. This increase in the remanence is a result of the dramatic decrease in the superparamagnetic contribution indicated in figure 7.

In addition to the changes in remanence characteristics there is also an associated increase in the coercivity of the particles as the median diameter increases, due to the reduced significance of the thermal energy relative to the anisotropy energy. Thus, the coercivity increases with increasing median particle diameter, as shown in figure 6.

As previously indicated for the larger particle systems in figure 6, the coercivity will also increase as the temperature is lowered, since an increase in D_v causes a corresponding increase in the energy barrier ($KV/4$) defined in (10). Thus by increasing the particle volume, or by lowering the temperature, the superparamagnetic magnetization contribution may become insignificant, compared to the total magnetization, signifying that the majority of particles are blocked for such configurations.

4.2. The variation of coercivity and remanence with temperature

The effects of temperature on the saturation remanence and coercivity of a fine-particle ensemble with cubic anisotropy has been investigated both in terms of the absolute temperature and through an examination of the temperature-related ratio D_p/D_v derived from (12).

The temperature-dependent variation of saturation remanence and coercivity for a system of particles with $D_v = 100$ Å, $K = 2 \times 10^6$ erg cc^{-1} and $I_s = 400$ emu cc^{-1} are shown in

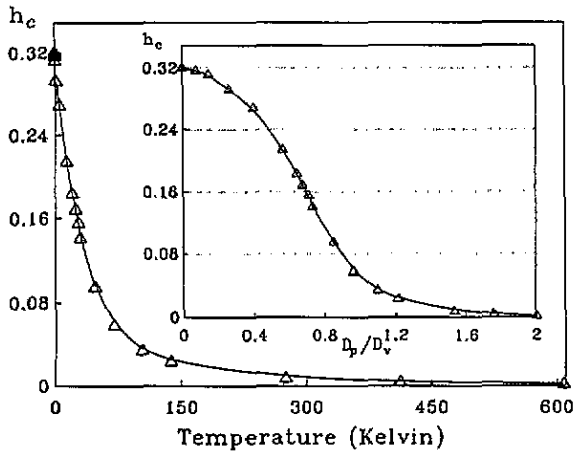

Figure 8. The effect of temperature on h_c for a system with cubic anisotropy, where $D_v = 100$ Å, $K = 2 \times 10^6$ erg cc^{-1}, $\sigma = 0.3$ and $I_s = 400$ emu cc^{-1}. Inset: the effect of D_p/D_v on h_c for a system with cubic anisotropy.

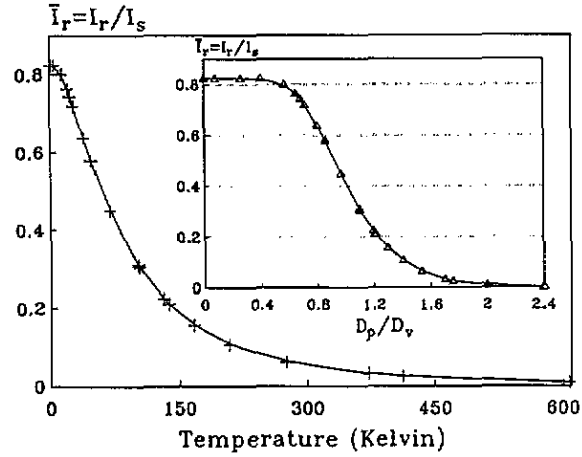

Figure 9. The effect of temperature on $\bar{I}_r$ for a system with cubic anisotropy, where $D_v = 100$ Å, $K = 2 \times 10^6$ erg cc^{-1}, $\sigma = 0.3$ and $I_s = 400$ emu cc^{-1}. Inset: the effect of D_p/D_v on $\bar{I}_r$ for a system with cubic anisotropy.

figures 8 and 9 respectively. The value of the standard deviation was kept constant at $\sigma = 0.3$.

The same data are expressed relative to the more general parameter D_p/D_v in the insets in figures 8 and 9. The insert in figure 8 indicates that as (D_p/D_v) increases the probability of thermally activated magnetization reversal increases, so the reduced coercivity, h_c, decreases. Beyond $D_p/D_v = 2$ the energy barriers are sufficiently reduced for magnetization changes to occur in very low reverse fields. Note that there is irreversible behaviour for median diameters significantly smaller than D_p as the most important consequence of the particle size distribution.

Similarly, the insert in figure 9 indicates that, for very small values of D_p/D_v, the fraction of superparamagnetic particles in the assembly is negligible and the optimum value

of remanence is achieved. The maximum value of $\bar{I}_r = 0.831$ begins to decrease beyond $D_p/D_v = 0.4$ as the superparamagnetic contribution to the magnetization increases.

4.3. The variation of remanence and coercivity with σ

Figures 10 and 11 illustrate the variations of the remanence and reduced coercivity as a function of the standard deviation of the particle size distribution at 200K. It has been assumed that a saturating field has been applied to the system of particles at each value of σ.

For the particle systems with largest median diameter, as σ approaches zero (when all the particles are of equal diameter) the maximum remanence and coercivity are achieved as the majority of particles are blocked (i.e. $h_c = 0.321$, $\bar{I}_r = 0.831$). This is not the case, however, for the particle assemblies with a small median diameter of the order of $D_v = 100\,\text{Å}$. In this configuration the particles are predominantly superparamagnetic ($y < y_p(0)$) and consequently both the remanence and coercivity tend towards zero as σ becomes smaller.

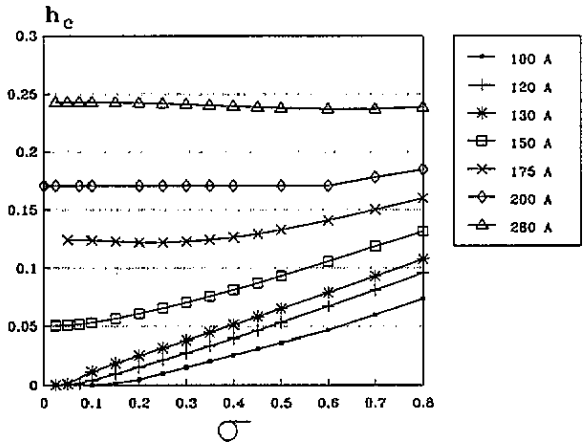

Figure 10. Variation of h_c against standard deviation of the particle size distribution σ.

5. Conclusions

In this paper we have comprehensively extended the original work of Joffe and Heuberger [4] on the hysteresis properties of assemblies of non-interacting single-domain particles with multiaxial anisotropy at 0 K. We have extended the theoretical treatment of such hysteresis loop calculations by considering the consequences of thermally activated magnetization reversal and by adopting a log-normal particle size distribution of particle diameters. This produces a model that is capable of realistic comparison with experimental data. In this paper we have shown the effects of mean particle diameter, standard deviation and temperature on the superparamagnetic and blocked components of the hysteresis loop and their consequences for the reduced coercivity and remanence.

The significance of the model is in its capability for direct comparison with experimental data. Such a detailed comparison might be expected to reveal information on particle

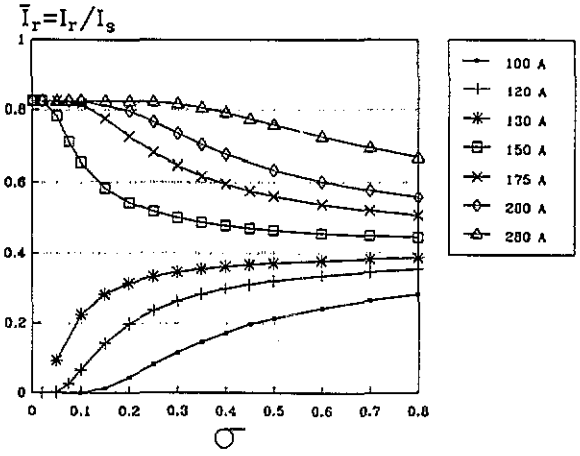

Figure 11. Variation of $\bar{I}_r$ against standard deviation of the particle size distribution σ.

interaction effects and incoherent reversal mechanisms, which may contribute to the behaviour of practical fine particle systems. In this respect two phenomena are important: the time dependence of the magnetization (which may provide information on magnetization reversal mechanisms) and the behaviour of the remanent magnetization (sensitive to interaction effects). These questions are addressed in the following paper.

References

[1] Stoner E C and Wohlfarth E P 1948 *Trans. R. Soc.* A **240** 599
[2] Gaunt P 1968 *Phil. Mag.* **17** 263
[3] Joffe I 1969 *J. Phys. C: Solid State Phys.* **2** 1537
[4] Joffe I and Heuberger R 1974 *Phil. Mag.* **314** 1051
[5] Geshev J, Popov O, Masheva V and Mikhov M 1990 *J. Magn. Magn. Mater.* **92** 185
[6] Geshev J and Mikhov M 1992 *J. Magn. Magn. Mater.* **104-107** 1569
[7] Street R and Woolley J C 1949 *Proc. Phys. Soc.* A **62** 562
[8] Nèel L 1949 *Ann. Geophys.* **5** 99
[9] Chantrell R W, O'Grady K, Bradbury A, Charles S W and Popplewell J 1985 *J. Phys. D: Appl. Phys.* **18** 2505
[10] Chantrell R W, O'Grady K, Bradbury A, Charles S W and Hopkins N 1987 *IEEE Trans. Magn.* **23** 204
[11] Bean C P and Livingston J D 1959 *J. Appl. Phys.* **30** 120S
[12] Abramovitz M and Stegun I 1964 *Handbook of Mathematical Functions* (Washington, DC: National Bureau of Standards) p 931